Nuclear Materials and Energy 24 (2020) 100771

Contents lists available at ScienceDirect

Nuclear Materials and Energy

journal homepage: www.elsevier.com/locate/nme

Effect of HIP at 800 and 900 °C on microstructure and properties of extruded Be-Ti composites

Ramil Gaisin[a,*], Vladimir Chakin[a], Michael Duerrschnabel[a], Rolf Rolli[a], Tobias Weingaertner[a], Aniceto Goraieb[b], Pavel Vladimirov[a]

[a] Karlsruhe Institute of Technology, Hermann-von-Helmholtz-Platz 1, 76344 Eggenstein-Leopoldshafen, Germany
[b] Karlsruhe Beryllium Handling Facility, Hermann-von-Helmholtz-Platz 1, 76344 Eggenstein-Leopoldshafen, Germany

ARTICLE INFO

Keywords:
Beryllide
Beryllium
Hot isostatic pressing
Extrusion
DEMO

ABSTRACT

Hot isostatic pressing (HIP) has been proposed for manufacturing large hexagonal $TiBe_{12}$ blocks for neutron multiplication in the new reference design of the DEMO blanket. This paper investigates the effect of HIP at 800 and 900 °C on the microstructure and the properties of extruded Be-Ti composites with the main aim of optimizing HIP parameters. Be-Ti composites produced by powder extrusion at 650 °C consist exclusively of Be and Ti phases. During HIP, they interact forming titanium beryllides with a volume fraction of 70–79%. These beryllides have a very high microhardness of 1130–1680 HV.

X-ray diffraction showed that the main beryllide phase is $TiBe_{12}$. After HIP at 900 °C, it has a very fine-grained microstructure with a mean grain size of 190 nm. Auger electron spectroscopy revealed that the $TiBe_2$ beryllide forms a thin layer surrounding the remaining Ti phase. Ti_2Be_{17} can be found at the prior titanium phase locations in the form of small particles. The titanium and beryllium phase do not dissolve completely during the used HIP process. In addition, the beryllium phase exhibited a higher porosity after HIP. This results in densities as low as 94.4% and 95.9% of the theoretical density of $TiBe_{12}$ after heat treatment at 800 °C and 900 °C, respectively.

Differential scanning calorimetry showed that beryllides are mainly synthesized in the temperature range of 670–740 °C, which can be monitored by the observation of a heat release. To accomplish diffusion processes in the Be-Ti composite, HIP should be carried out at temperatures exceeding 900 °C. Heating rates should be less than 10 K/min to avoid excessive overheating.

1. Introduction

Compared to pure Be, the intermetallic titanium beryllide $TiBe_{12}$ has an increased operating temperature, higher corrosion resistance, swells less and retains a lower amount of tritium under neutron irradiation [1–6]. According to the new reference design of the blanket of the demonstration nuclear fusion reactor power plant (DEMO), solid titanium beryllide blocks having a size of Ø144 mm × 150 mm are to be used for neutron multiplication [1]. A scalable technology for the production of such blocks should be developed to prove the feasibility of manufacturing titanium beryllide in industrial quantities. Preliminary experiments showed that conventional casting of $TiBe_{12}$ results in relatively low quality ingots with high porosity and variations in composition caused by partial evaporation of beryllium [3,7]. In case of powder metallurgy route, various methods for the manufacture of beryllides samples have been tested: hot isostatic pressing (HIP) [7–8], vacuum hot pressing (VHP) [9–11], and spark plasma sintering (SPS) [12–13]. Among them, HIP is known to provide a fine-grained $TiBe_{12}$ structure with reasonable mechanical properties [7,14–15]. However, the synthesis of beryllides is accompanied by a substantial heat release, which can lead to the melting of the capsule and damage of the HIP equipment if not properly taken into account. On the other hand, the synthesis of $TiBe_{12}$ is incomplete at too low HIP temperatures. Therefore, the HIP parameters for the synthesis of titanium beryllides should be optimized before fabrication on industrial scales.

In the present work, extruded rods of Be-Ti composites were subjected to HIP at temperatures of 800 °C and 900 °C. Extrusion was chosen for the compaction of Be and Ti powders because a scale-up is easily possible and it results in a high density material. The work presented below was aimed to determine the interaction behavior of Be and Ti phases in an extruded composite and the formation of titanium beryllides. This can foster the definition of HIP conditions for large-scale beryllide block production for DEMO.

* Corresponding author.

https://doi.org/10.1016/j.nme.2020.100771
Received 2 April 2020; Received in revised form 17 June 2020; Accepted 24 June 2020
Available online 30 June 2020

2. Materials and experimental techniques

Pure Be and Ti powders were blended together, sealed into capsules, and extruded at 650 °C with reduction ratio of 8:1 at the Extrusion Research and Development Center, Technical University of Berlin. Extrusion details have been previously described in [16]. The target composition was $TiBe_{12}$ (Be-7.7 at.% Ti or Be-30.8 wt% Ti). The chemical composition of the extruded composite was measured as follows in wt.%: Be-29.11Ti-0.219O-0.102Fe-0.077C-0.037Al-0.036 Mg-0.022Si-0.0018 N-0.0018Ca-0.00193U [7]. After hot extrusion, sections of Be-Ti rods having Ø40mm × 12 mm were sealed into capsules and subjected to HIP at temperatures of 800 and 900 °C under argon pressure of 102 MPa for 4 h in the "Edmund Buehler HIP 2000" at the Karlsruhe Beryllium Handling Facility (KBHF). The samples were heated and cooled at a rate of about 10–20 K/min.

After HIP, Be-Ti samples were removed from the capsules and cut with a diamond saw along and across the extrusion direction. Sample surfaces were polished either mechanically or electrolytically after sequential mechanical grinding. The samples were investigated using scanning electron microscopy (SEM) on a Zeiss Merlin microscope. Energy-dispersive X-ray spectroscopy (EDS) was used to build elemental maps of Ti, O, C, Al, N, and Si. Auger electron spectroscopy (AES) was performed on a PHI 710e/680 Hybrid Nanoprobe to analyze the content of Be, Ti, and C. The volume fraction of the phases was determined by the systematic point count method using mechanically polished samples.

Electron-transparent lamellae were prepared by focused ion beam (FIB) on a Zeiss Auriga CrossBeam system and were examined using a Talos F200X transmission electron microscope equipped with a Super X-EDS system for energy-dispersive X-ray spectroscopy (EDS), a Gatan Infineon electron energy loss spectrometer (EELS), and a scanning unit (STEM) with high-angle annular dark-field (HAADF) detector.

Differential scanning calorimetry (DSC) was performed to analyze the synthesis of titanium beryllide on a Netzsch STA 449 F3 Jupiter. To do this, samples of extruded Be-Ti composite of about 60 mg were heated up to 1000 °C in an argon gas flow at a rate of 10 K/min. X-ray diffraction (XRD) measurements were performed on a Seifert PAD II diffractometer with Cu-K$\alpha_{1/2}$ radiation. Microhardness was measured on a Zwick Roell Indentec ZHμ tester using indentation forces of 100–1000 gf. Density was measured by the hydrostatic weighing in $C_{14}H_{30}$ liquid media (Mettler Toledo MS303TS). The density of pure $TiBe_{12}$ of 2.288 g/cm^3 was used to calculate the percentage of theoretical density (TD) of the samples after HIP [17].

3. Results and discussion

3.1. Microstructure

Fig. 1 compares the XRD patterns of the Be-Ti composite material after extrusion and after subsequent HIP at 800 °C and 900 °C. The extruded material consists of pure Be and Ti phases (Fig. 1a), whereas several titanium beryllide phases are present after HIP (Fig. 1b and c). In SEM micrographs, titanium is identified as bright fibers elongated along the extrusion direction (Fig. 2a), and Be is represented by the surrounding dark matrix. Cross sections (Fig. 2b) revelaed that the Ti-fibers have an irregular shape. The extruded Be-Ti composite was described in detail in a previous work [7]. Extrusion resulted in a relatively high density of 2.204 g/cm3 or 97.6% of the TD of the corresponding Be-30.8wt.%Ti composite (Table 1).

After extrusion and HIP at 800 °C, strong $TiBe_{12}$ peaks appeared on the XRD pattern (Fig. 1b) while intensities of the Ti and Be peaks decreased. Note that intermediate beryllide phases, $TiBe_2$ and Ti_2Be_{17}, have very low peak intensities presumably due to their low volume fraction. The volume fraction of the Be matrix and the Ti fibers significantly decreased to 25% and 5%, respectively (Table 1). During HIP, the Be and Ti phases interacted and formed vast gray areas with a

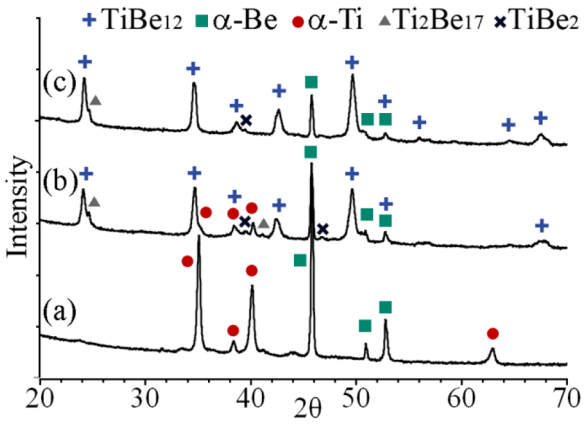

Fig. 1. X-ray diffraction patterns: (a) extruded Be-Ti composite, and after subsequent hot isostatic pressing at (b) 800 °C, and (c) 900 °C.

volume fraction of 70% (Fig. 2c,d). In the cross sections, these regions often have a flower-like shape consisting of a Ti core and beryllide "petals" (Fig. 2d). Such structures were also observed in Be-Ti composite material after SPS at lower temperatures or insufficient sintering time [12,19]. Since the peak intensities of the $TiBe_{12}$ phase observed in the XRD pattern are dominating compared to other beryllides (Fig. 1b), these gray areas should correspond to the $TiBe_{12}$ phase containing only traces of other beryllides. According to Be-Ti phase diagram [14,18], these intermediate beryllide phases should lie between the Ti and the $TiBe_{12}$ phases. However, they do not form identifiable layers in SEM micrographs. Compared to the material after extrusion, a considerable reduction in the size of titanium particles is evident. The phase boundary of Ti and the beryllide phase is uneven and has protrusions along the extrusion direction (Fig. 2c). This is attributed to the growth of the beryllide phase towards the titanium phase. The protrusions at the Be / $TiBe_{12}$ phase boundary are better identified across the extrusion direction in the form of beryllide "petals" of the flower-like structures (Fig. 2d).

After HIP at 900 °C, the amount of $TiBe_{12}$ increases, whereas the peaks of Be, $TiBe_2$, and Ti_2Be_{17} decrease in the XRD pattern (Fig. 1c). The peaks of the Ti phase are weak and cannot be detected reliably on the XRD pattern (Fig. 1c). In micrographs (Fig. 2f, e), the titanium phase is still present with a volume fraction of about 1%. The titanium particles mostly dissolved, leaving a number of fine particles in the center of the flower-like structures (Fig. 2e, f, light gray particles). The morphology of these fine particles is very similar to the morphology of the Ti_2Be_{17} phase [12,19–21]. Note that after HIP at 800 °C, the number of such Ti_2Be_{17} particles is much smaller compared to HIP at 900 °C. Some of those particles were detected only close to the Ti phase across extrusion direction (Fig. 2d). In general, the microstructures after HIP at 800 °C and 900 °C are similar and differ mainly in the volume fractions of the constituent phases. The volume fraction of the beryllide phases (mostly $TiBe_{12}$) reaches 79% (Table 1). Gray beryllide areas are often "separated" by stripes of BeO (Fig. 2e). These oxides were inherited from the beryllium phase and represent prior particle boundaries [7,15].

The Be phase has a higher porosity after the HIP process, which can be attributed to the Kirkendall effect due to the difference in diffusion rates of beryllium and titanium atoms. A similar increase of porosity in beryllium was also observed previously [7,22]. In $TiBe_{12}$, small pores are also observed near the beryllide / Be phase boundary, which apparently formed by the growth of beryllide towards the porous beryllium phase (Fig. 2e). An increase in porosity after the HIP process was also determined by density measurements. The densities after treatment at 800 °C and 900 °C are 2.159 g/cm^3 and 2.195 g/cm^3, respectively, which are lower than after extrusion, which resulted in 2.204 g/cm^3 (Table 1). Compared with TD of $TiBe_{12}$, HIP at 800 °C and 900 °C results

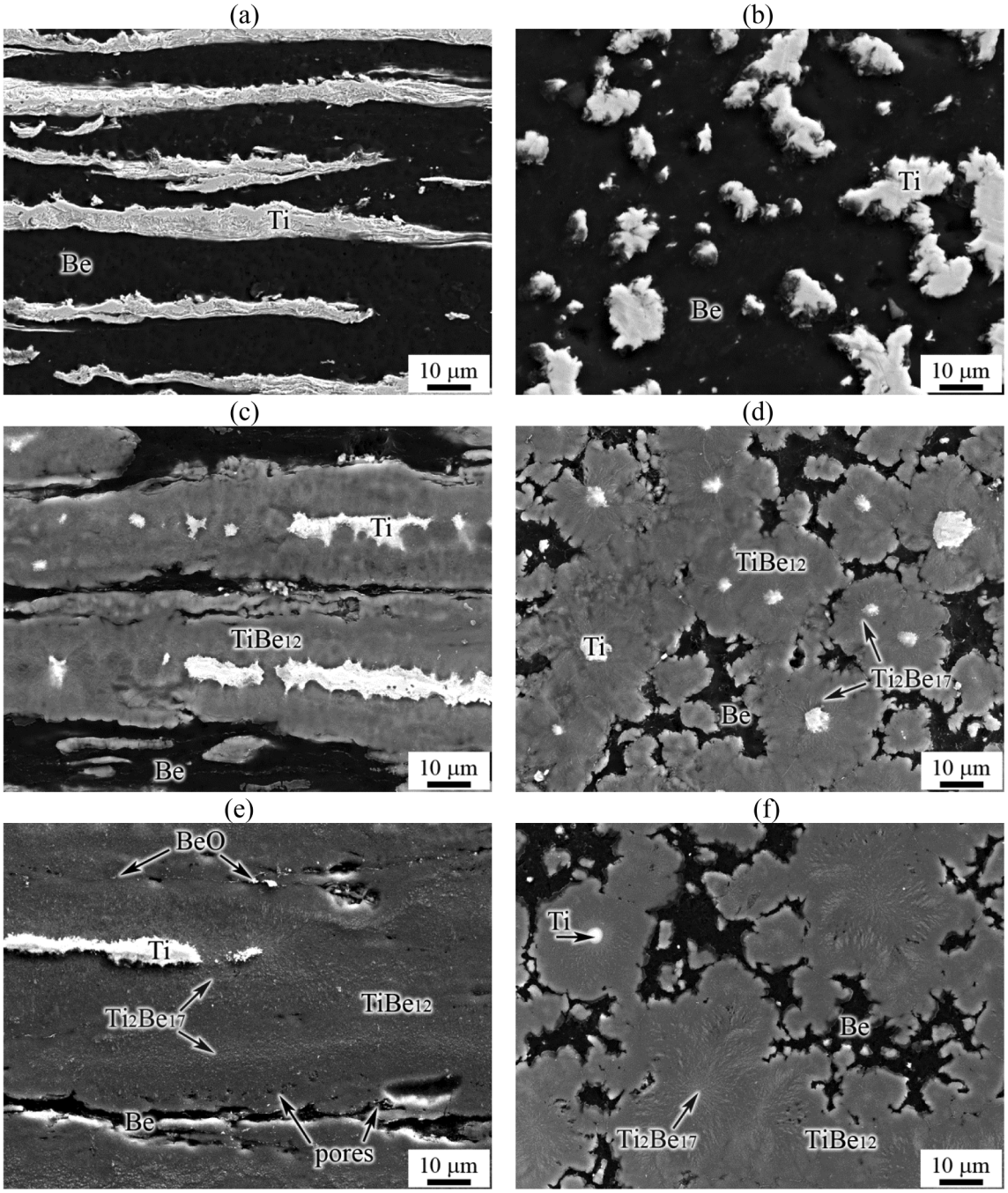

Fig. 2. Microstructure of Be-Ti as studied by SEM: (a, b) after extrusion, and after subsequent hot isostatic pressing at (c, d) 800 °C, (e, f) 900 °C; (a, c, e) along and (b, d, f) across extrusion direction. In (a, c, e), the extrusion direction is horizontal.

Table 1
Density, phase composition, volume fraction and microhardness of Be-Ti composites depending on the processing.

Processing, °C	Density, g/cm^3	Phase	Volume fraction, %	Microhardness, HV 0.1
Extrusion	2.204	Be	79	320 ± 20
		Ti	21	315 ± 20
Extrusion + HIP at 800 °C	2.159	Beryllides	70	1130 ± 200
		Be + porosity	25	370 ± 30
		Ti	5	–
Extrusion + HIP at 900 °C	2.195	Beryllides	79	1680 ± 100
		Be + porosity	20	370 ± 30
		Ti	1	–

in 94.4% and 95.9% density, respectively.

Energy dispersive X-ray and Auger electron spectroscopies were used for the further study of the material after extrusion and HIP. Fig. 3 shows SEM micrograph and EDS elemental maps of a flower-like structure with a titanium core and beryllide “petals” in the Be-Ti composite after extrusion and HIP at 800 °C. Beryllium cannot be reliably detected by EDS, since its low energy characteristic X-ray is mostly absorbed by the sample. The titanium elemental map confirms the highest Ti content in the center and the absence of Ti in the surrounding Be matrix (Fig. 3b). The EDS map shows a blur at the maximum of titanium, which extends beyond the boundaries of the titanium phase in the SEM micrograph. On the corresponding linear Ti profile (Fig. 3b), the inclined boundaries of the Ti core are visible. This might be an indication of the presence of intermediate beryllide phases with a

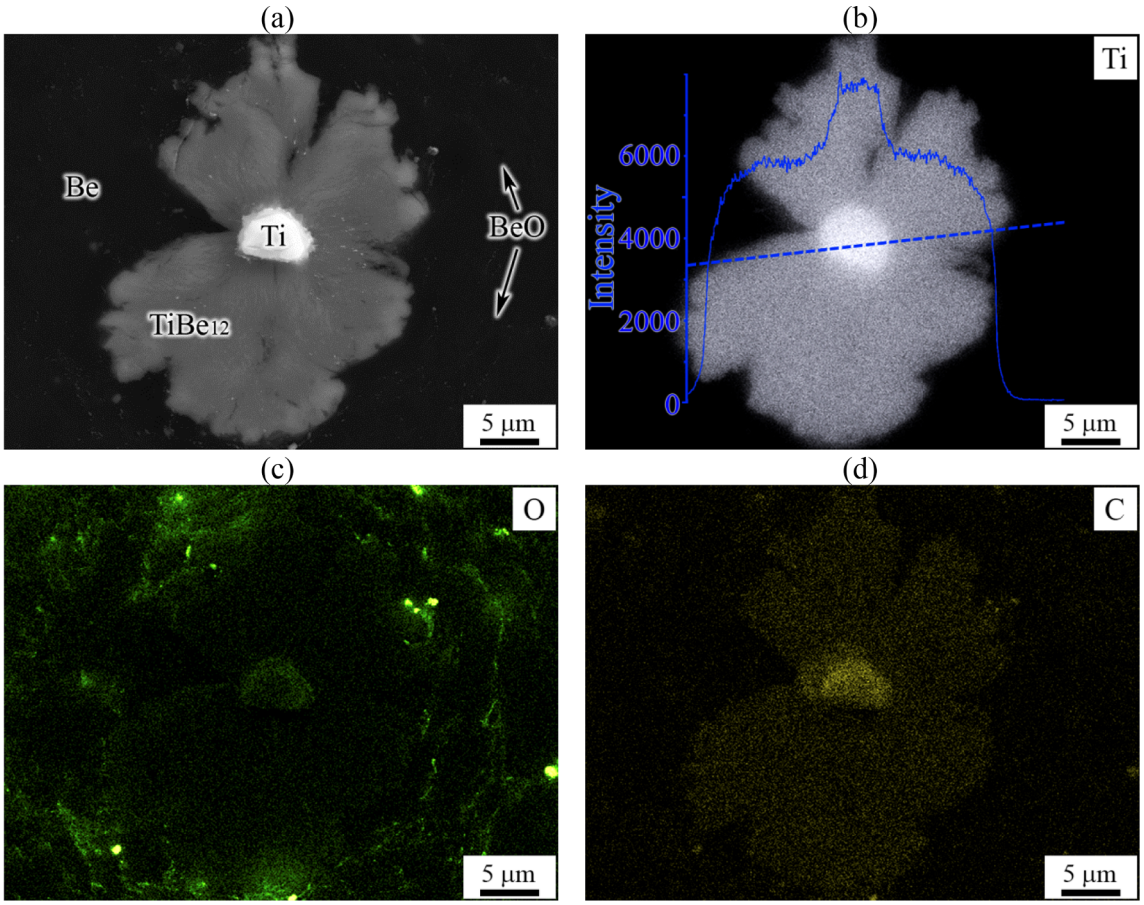

Fig. 3. Flower-like structure in Be-Ti composite after extrusion and hot isostatic pressing at 800 °C: (a) SEM picture, (b-d) elemental EDS maps: (b) titanium map with corresponding Ti profile along the dashed blue line, (c) oxygen, (d) carbon.

higher Ti content, i.e. $TiBe_2$ and Ti_2Be_{17}. Oxygen is mainly distributed in Be in the form of concentric circles of particles (Fig. 3c). Such stripes with BeO particles inside the beryllium phase were observed earlier in the extruded Be-Ti composite and represent the prior particle boundaries [2]. Many other impurities, such as C (Fig. 3d), Al, Si, N are preferentially concentrated in the beryllides and in the titanium phase.

Fig. 4 shows the results of Auger electron spectroscopy of a longitudinal section of a titanium-rich area after extrusion and HIP at 900 °C. The beryllium elemental map shows the absence of Be inside the core of the titanium-rich particle (Fig. 4b). The intermediate beryllide phase, which was identified as $TiBe_2$, has lower Be and higher Ti content compared to the other beryllide phases (Fig. 4b, red color) and was found to surround the Ti phase. The Ti_2Be_{17} phase was not reliably detected in Be and Ti elemental maps, presumably due to its close chemical composition with $TiBe_{12}$.

Outside of $TiBe_2$, a layer with higher carbon and low Be and Ti content was observed. The reason for the formation of such a layer is not yet clear. The carbon content of the extruded composite is only about 0.08 wt%, but carbon can be concentrated at the $TiBe_{12}$ / $TiBe_2$ or Ti_2Be_{17} boundaries by displacing carbon atoms from the $TiBe_{12}$ phase during its growth towards the Ti phase. Note that EDS also showed a higher content of C (Fig. 3d), Al, Si, N in the area with a high titanium content. Such high concentration of impurities may also "protect" the Ti phase from its further dissolution in $TiBe_{12}$.

Focused ion beam was used to lift out a lamella from the $TiBe_{12}$ phase in Be-Ti composite after extrusion and HIP at 900 °C. Fig. 5 represents results of a TEM investigation. The microstructure is formed by a number of fine grains having a size ranging in between 40 and 900 nm (Fig. 5a). The average grain size was determined to be 190 ± 90 nm. The electron diffraction pattern (Fig. 5d) confirmed the polycrystalline structure of the $TiBe_{12}$ phase. The STEM-EDS analysis showed a slightly lower Ti content on grain boundaries (Fig. 5b). Beryllium (confirmed by STEM-EELS) and impurity elements are distributed quite homogeneous. Only the Si elemental map showed several small particles with a higher Si content located at the $TiBe_{12}$ grain boundaries (Fig. 5c).

Another lamella was lifted out from a flower-like structure as in Fig. 3. The surface of the lamella is parallel to the extrusion direction and shows part of a longitudinal section of the flower-like structure. Fig. 6a represents a panoramic view of the lamella with the Ti phase in the left side, the $TiBe_{12}$ phase in the middle, and the Be phase in the right side. The superimposed Ti EDS profile confirmed the absence of titanium in the Be phase. The $TiBe_{12}$ phase has a fine-grained microstructure, while the Be and Ti phases have much larger grains. No intermediate phases were found between $TiBe_{12}$ and Be. A sloping decrease in the intensity of titanium at the $TiBe_{12}$ and Be interface is caused by a partial superposition of these phases. Fig. 6b shows an increased view of Ti and $TiBe_{12}$ interface with two distinct layers. EDS (Fig. 6c), EELS, and diffraction (not shown in the work) in TEM confirmed that the first layer adjacent to the titanium phase is formed by the $TiBe_2$ phase, and the second layer adjacent to $TiBe_{12}$ is formed by Ti_2Be_{17}. Other possible beryllide phases such as $TiBe_3$, $TiBe_5$, $TiBe_{10}$, Ti_2Be_{13} or Ti_4Be_5 were not found in the microstructure. $TiBe_2$ grains have an elongated shape with a long axis along the Ti boundary. Ti_2Be_{17} grains are larger and have a more equiaxed shape. Both phases $TiBe_2$ and Ti_2Be_{17} have a number of defects such as stacking faults and twins. EDS also showed a higher content of Si (Fig. 6d), Al, C, N in the Ti, $TiBe_2$ and Ti_2Be_{17} phases compared to $TiBe_{12}$. More silicon was detected at the interface of Ti_2Be_{17} and $TiBe_{12}$ (Fig. 6d). Apparently, silicon cannot dissolve much in $TiBe_{12}$ and forms Si-rich particles, also found in Fig. 5d.

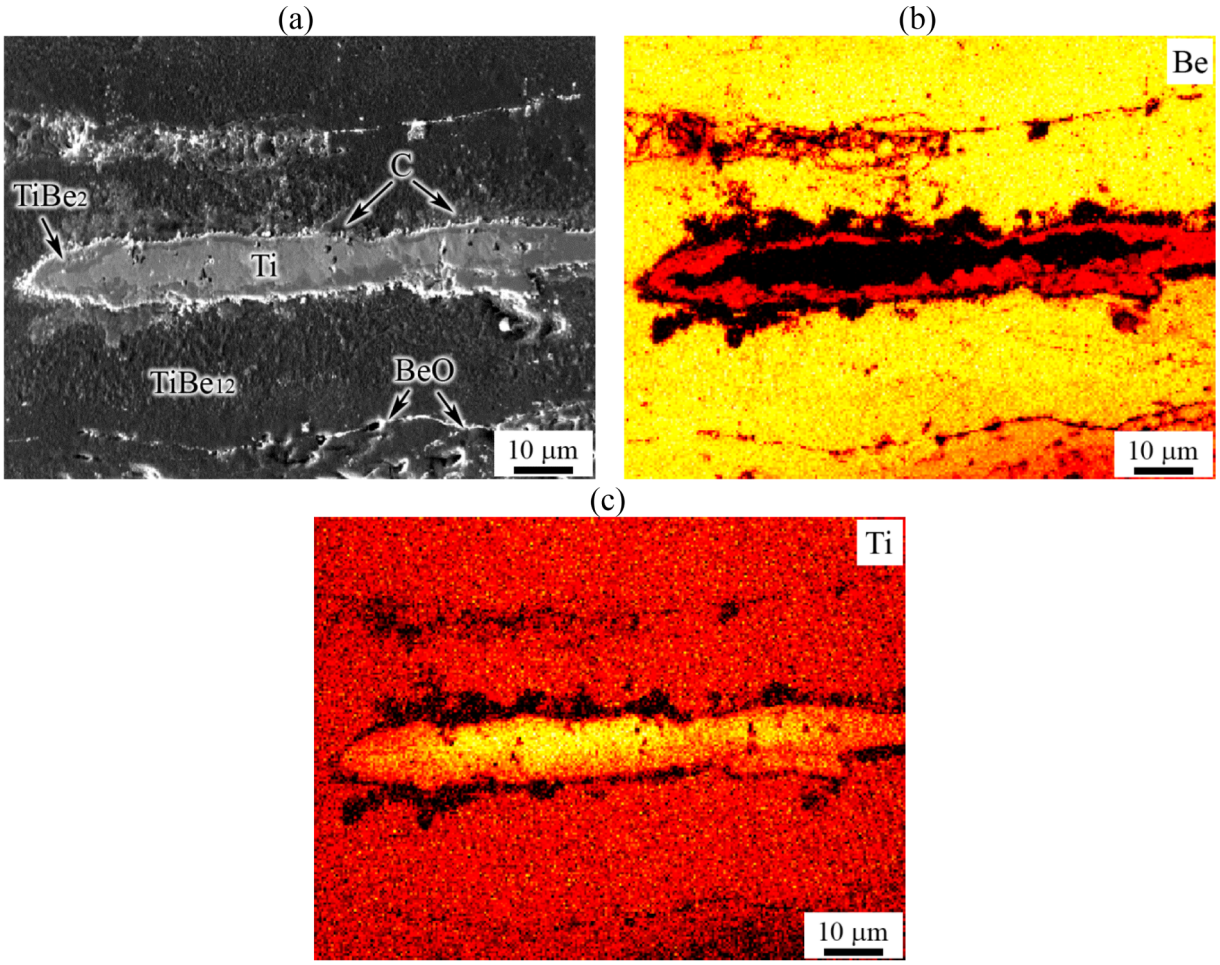

Fig. 4. Longitudinal section of Ti-rich area in Be-Ti composite after extrusion and hot isostatic pressing at 900 °C: (a) SEM picture, (b–c) elemental Auger electron spectroscopy maps: (b) beryllium, (c) titanium.

Such a fine-grained structure of titanium beryllide was observed earlier after extrusion and HIP at 1100 °C [7]. However, the higher HIP temperature resulted in a larger grain size in the range of 0.3–2.5 μm. The grain boundaries were often pinned by a number of very fine particles of BeO. After HIP at 900 °C, such small uniformly distributed oxide particles were not found. Most of the oxygen is still concentrated in the beryllium phase and not in $TiBe_{12}$ (Fig. 3c). With the dissolution of the Be phase at higher HIP temperatures, more oxides can enter the beryllide phase and inhibit grain boundary movement. The reason for the small grain size of $TiBe_{12}$ after HIP at 900 °C remains unclear. Since Ti has a low solubility in Be [14], their interaction can begin by the penetration of Be atoms into the Ti phase and the formation of $TiBe_2$. The existence of the Ti_2Be_{17} phase is essential for the formation of $TiBe_{12}$, since Ti_2Be_{17} appears only at the boundary of Be and $TiBe_2$, which subsequently leads to the formation of $TiBe_{12}$ at the Be/Ti_2Be_{17} phase boundary. The complexity of the diffusion reaction sequence can lead to a complete rearrangement of Be and Ti lattices and the formation of a fine-grained $TiBe_{12}$ structure. In [15] the small grain size in VBe_{12} after HIP was explained by incomplete recrystallization, resulting from the low consolidation temperature. However, even an increase in HIP temperature from 900 °C to 1100 °C in Be-Ti composite does not lead to extensive grain growth.

3.2. Microhardness

In the extruded Be-Ti, the beryllium and titanium phases have a similar microhardness of about 315–320 HV (Table 1). After HIP at 800 °C, the beryllide phase shows a much higher microhardness with a large scatter in hardness values, 1130 ± 200 HV, while the beryllium phase (including pores) has a microhardness of 370 ± 30 HV. It was not possible to measure the microhardness of the titanium phase after HIP due to its small volume fraction and small size. After HIP at 900 °C, the beryllide has a very high microhardness, 1680 ± 100 HV, and the microhardness of the Be phase remains low, 370 ± 30 HV.

Vacuum-hot-pressed $TiBe_{12}$ has a hardness of 960 HV [3,11]. The increased hardness after HIP at 800 °C and especially at 900 °C can be explained by the small grain size, due to the low treatment temperature, as well as the presence of other beryllide phases, such as Ti_2Be_{17} and $TiBe_2$. A strong increase in microhardness from 1130 HV at 800 °C to 1680 HV at 900 °C HIP temperature can be associated with an increased amount of the Ti_2Be_{17} phase, as well as with a decrease in the porosity of the beryllide phase during HIP at a higher temperature. A higher hardness of the Ti_2Be_{17} phase compared to the $TiBe_{12}$ phase was reported in [4]. Further HIP temperature increase up to 1100 °C led to a larger grain size and a decrease in microhardness to 1420 HV [7].

3.3. Differential scanning calorimetry

Fig. 7 shows a part of a differential scanning calorimetry curve for heating of an extruded Be-Ti sample. In the temperature range of 667–810 °C, an exothermic peak is observed. Since neither Be nor Ti have phase transformations in this temperature range, the peak can be only caused by the synthesis of beryllides. The main synthesis reaction begins at 667 °C and ends at 743 °C. Small peaks are also observed on the DSC curve up to the highest measurement temperature, 1000 °C. Apparently, the synthesis reaction does not end at 743 °C, but continues

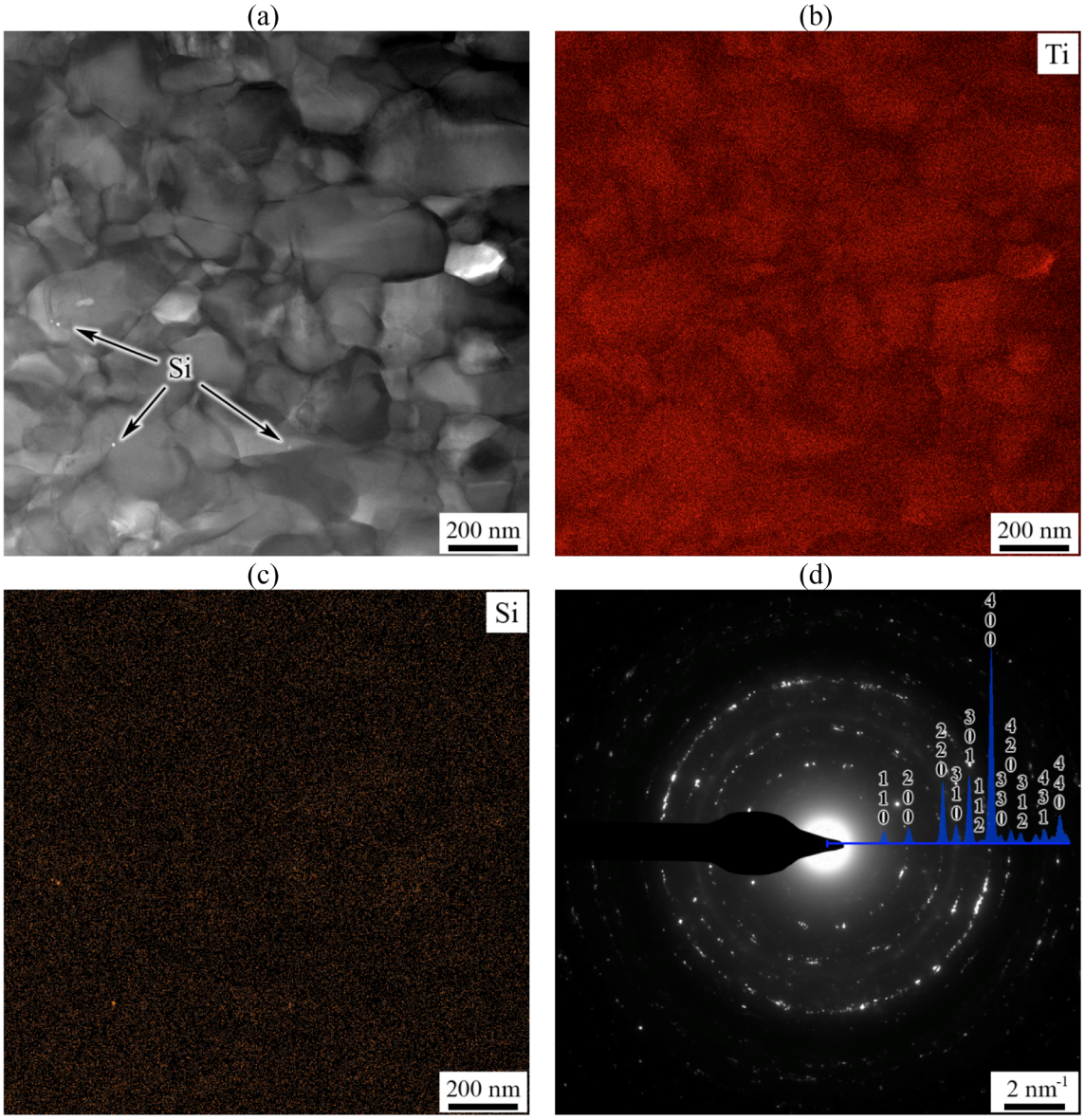

Fig. 5. Microstructure of $TiBe_{12}$ in Be-Ti composite after extrusion and hot isostatic pressing at 900 °C: (a) high-angle annular dark-field image, (b) Ti elemental EDS map, (c) Si elemental EDS map, (d) selected area electron diffraction pattern from the same region with the designation of the corresponding $TiBe_{12}$ planes.

with temperature increase in other places where beryllium and titanium have not yet reacted. Thus, there is a rapid increase in the amount of beryllides when heated up to 650–800 °C, and a slight additional increase in the amount of beryllides in the range of 800–900 °C (Table 1). A phase transformation peak of α-Ti to β-Ti was not observed probably due to the small volume fraction of the remaining titanium after the synthesis of beryllides.

The thermal effect of the main reaction of Be and Ti at 667–743 °C was calculated as 63.1 J/g (Fig. 7). This is significantly less than the heat of fusion of beryllium or titanium with 1355 and 322 J/g, respectively [14]. To evaluate whether the thermal effect of reaction between Be and Ti can lead to overheating and partial melting of the composite or beryllide, we assume that this reaction simultaneously heats the extruded composite Be-Ti (an extreme case). Then the temperature difference before and after heating, ΔT, can be calculated as follows:

$$\Delta T = Q/c_p(\text{Be} - \text{Ti})\cdot \quad (1)$$

where Q = 63.1 J/g is the thermal effect of the reaction of Be and Ti (Fig. 6); c_p(Be-Ti)·is the specific heat capacity of the extruded Be-30.8Ti (wt.%). The latter can be determined as:

$$c_p(\text{Be} - \text{Ti}) = 0.692 \times c_p(\text{Be}) + 0.308 \times c_p(\text{Ti}) \quad (2)$$

where c_p(Be) = 1.827 J/g/K and c_p(Ti) = 0.524 J/g/K [14] are cpecific heat capacities of Be and Ti, respectively.

This estimate using expressions (1) and (2) shows that the exothermic reaction of Be and Ti can only heat the extruded material by 44 K. However, the fast heating of the extruded material to higher temperatures can lead to the rapid synthesis of larger volume of titanium beryllides with greater thermal effect and overheating. The latter was observed during argon-arc melting of the extruded Be-30.8Ti (wt.%), when the initial heating of the composite up to the beginning of melting initiated a spontaneous reaction of beryllium and titanium, proceeding without additional heat supply [7]. Thus, the heating rate during HIP should not be higher than 10 K/s in order to avoid excessive overheating and damage to HIP equipment.

The results obtained indicate that the main synthesis of beryllides occurs at temperatures in the range of 670–740 °C. After HIP at 900 °C, the material still contains a significant amount of porous beryllium phase, traces of the titanium phase and other beryllide phases, i.e. $TiBe_2$

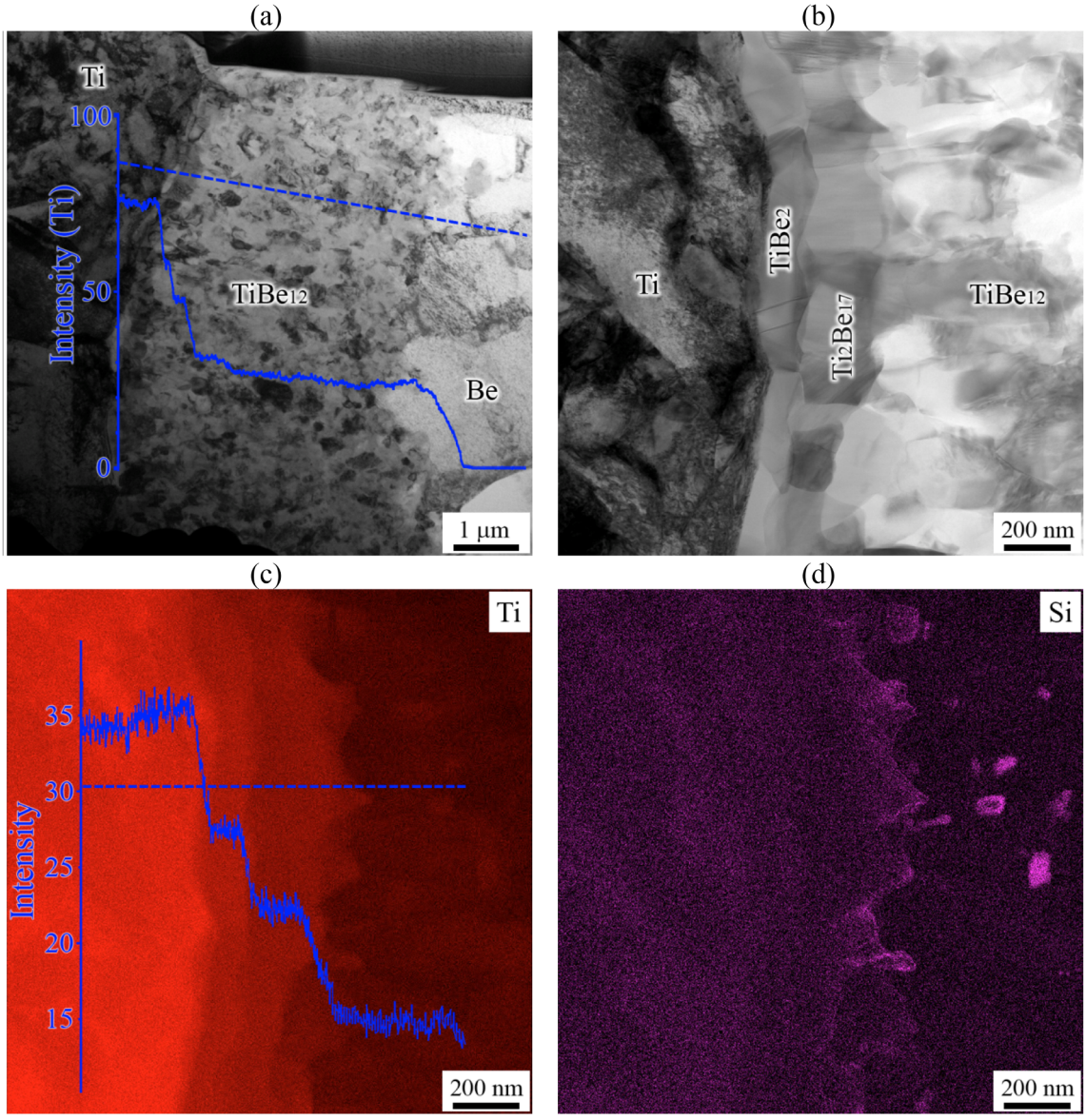

Fig. 6. Microstructure of the longitudinal section of a flower-like structure in Be-Ti composite after extrusion and hot isostatic pressing at 900 °C: (a) TEM panoramic view, (b) high-angle annular dark-field image of Ti and $TiBe_{12}$ interface, (c) Ti elemental EDS map, (d) Si elemental EDS map. In (a, c), corresponding Ti EDS profile along the dashed blue line is superimposed.

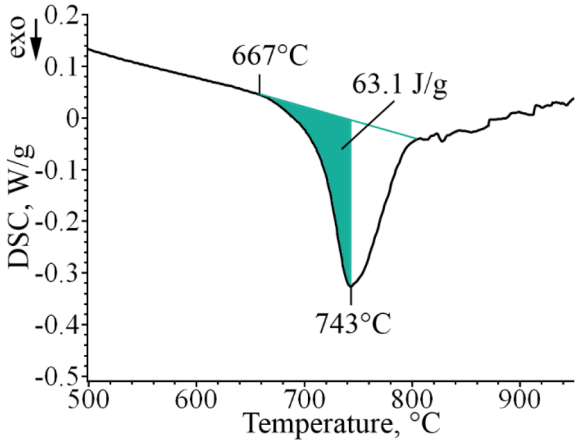

Fig. 7. A fragment of a differential scanning calorimetry (DSC) curve for heating of extruded Be-Ti sample, showing a strong exothermic peak at 667–810 °C.

and Ti_2Be_{17}. Thus, the phase transformations in material after HIP at 800 °C and 900 °C are not completed. The relatively low density indicates that the temperature of 800–900 °C is too low to reduce porosity by the applied HIP pressure. The higher porosity and presence of the beryllium phase are unacceptable for a blanket application in DEMO, since a higher amount of tritium can be retained under neutron irradiation. Therefore, HIP should be carried out at higher temperatures. Heating rates during HIP should not be faster than 10 K/min to avoid excessive overheating. The effect of HIP at 1000–1200 °C on the structure and properties of Be-Ti composites will be presented in a follow-up work.

4. Conclusions

Be-Ti composites were studied after extrusion and subsequent hot isostatic pressing (HIP) at 800 °C and 900 °C. The extruded composite material consists of pure Be and Ti phases. During HIP, beryllium and titanium interact and form titanium beryllides, mainly $TiBe_{12}$. The volume fraction of the beryllides reaches 70% and 79% after HIP at

800 °C and 900 °C, respectively. Differential scanning calorimetry showed that the beryllides are synthesized mainly in a temperature range of 670–740 °C. They continue to be synthesized at least up to 1000 °C. The synthesis is accompanied by a heat release capable to overheat the Be-Ti composite material by about 44 K.

The interaction of beryllium and titanium results in the formation of flower-like structures with an undissolved titanium core, beryllide "petals" and a beryllium periphery. Auger electron spectroscopy showed that a $TiBe_2$ layer surrounds the titanium phase. Ti_2Be_{17} can often be found at the former titanium phase locations in the form of numerous small particles. The main beryllide phase, i.e. $TiBe_{12}$, has a very fine-grained microstructure with a mean grain size of about 190 nm after HIP at 900 °C. It was also found that the beryllides exhibit high microhardness values in the range of 1130–1680 HV.

The beryllium phase does not dissolve completely during the HIP process and has a higher porosity. This results in relatively low densities of 94.4% and 95.9% of the theoretical density of $TiBe_{12}$ after treatment at 800 °C and 900 °C, respectively. HIP should be carried out at temperatures exceeding 900 °C, while keeping the heating rate at values less than 10 K/min to decrease the amount of porous beryllium and to avoid excessive overheating.

Declaration of Competing Interest

The authors declare that they have no known competing financial interests or personal relationships that could have appeared to influence the work reported in this paper.

CRediT authorship contribution statement

Ramil Gaisin: Scanning electron microscopy, Metallography, Writing, Visualization. **Vladimir Chakin:** Supervision, Validation. **Michael Duerrschnabel:** TEM Investigations, Writing. **Rolf Rolli:** Supervision, Differential scanning calorimetry, Microhardness. **Tobias Weingaertner:** Auger electron spectroscopy. **Aniceto Goraieb:** Supervision, Methodology of hot extrusion, Hot isostatic pressing. **Pavel Vladimirov:** Conceptualization, Supervision, Funding acquisition.

Declaration of Competing Interest

The authors declare that they have no known competing financial interests or personal relationships that could have appeared to influence the work reported in this paper.

Acknowledgements

This work has been carried out within the framework of the EUROfusion Consortium and has received funding from the Euratom research and training programme 2014–2018 and 2019–2020 under grant agreement No 633053. The views and opinions expressed herein do not necessarily reflect those of the European Commission.

References

[1] F.A. Hernández, P. Pereslavtsev, G. Zhou, B. Kiss, Q. Kang, H. Neuberger, V. Chakin, R. Gaisin, P. Vladimirov, L.V. Boccaccini, G.A. Spagnuolo, S. D'Amico, I. Moscato, Advancements in the helium-cooled pebble bed breeding blanket for the EU DEMO: holistic design approach and lessons learned, Fusion Sci. Technol. 75 (2019) 352–364.
[2] H. Kawamura, E. Ishitsuka, K. Tsuchiya, M. Nakamichi, M. Uchida, H. Yamada, K. Nakamura, H. Ito, T. Nakazawa, H. Takahashi, S. Tanaka, N. Yoshida, S. Kato, Y. Ito, Development of advanced blanket materials for a solid breeder blanket of a fusion reactor, Nucl. Fusion 43 (2003) 675–680.
[3] Y. Mishima, N. Yoshida, H. Kawamura, K. Ishida, Y. Hatano, T. Shibayama, K. Munakata, Y. Sato, M. Uchida, K. Tsuchiya, S. Tanaka, Recent results on beryllium and beryllides in Japan, J. Nucl. Mater. 367–370 (2007) 1382–1386.
[4] J.-H. Kim, M. Nakamichi, Comparative study on arc-melted and plasma-sintered beryllides, J. Alloy. Compd. 546 (2013) 171–175.
[5] J.-H. Kim, M. Nakamichi, Thermal analyses of beryllide pebbles in water vapor atmosphere as advanced neutron multipliers, Fusion Eng. Des. 124 (2017) 805–808.
[6] J. Shimwell, L. Lu, Y. Qiu, P. Pereslavtsev, A. Häußler, F. Hernández, C. Zeile, T. Eade, G.A. Spagnuolo, S. McIntosh, L. Packer, T. Barrett, Automated parametric neutronics analysis of the Helium Cooled Pebble Bed breeder blanket with Be12Ti, Fusion Eng. Des. 124 (2017) 940–943.
[7] R. Gaisin, V. Chakin, R. Rolli, J. Hoffmann, H. Leiste, T. Bergfeldt, U. Jäntsch, M. Klimenkov, J. Lorenz, A. Goraieb, P. Vladimirov, A. Möslang, Synthesis of $Be_{12}Ti$ compound via arc melting or hot isostatic pressing, J. Alloy. Compd. 818 (2020) 152919.
[8] P. Kurinskiy, V. Chakin, A. Moeslang, R. Rolli, A.A. Goraieb, H. Harsch, E. Alves, N. Franco, Characterisation of titanium beryllides with different microstructure, Fusion Eng. Des. 84 (2009) 1136–1139.
[9] S.M. Bruemmer, B.W. Arey, J.L. Brimhall, J.P. Hirth, Hot-hardness comparisons among isostructural $Be_{12}X$ intermetallic compounds, J. Mater. Res. 8 (7) (1993) 1550–1557.
[10] L.A. Jacobson, R.J. Hanrahan Jr., J.L. Smith, Beryllides, Intermetallic Compounds – Principles and Practice, John Wiley & Sons, Ltd, 2002, pp. 37–51.
[11] C.K. Dorn, W.J. Haws, E.E. Vidal, A review of physical and mechanical properties of titanium beryllides with specific modern application of $TiBe_{12}$, Fusion Eng. Des. 84 (2009) 319–322.
[12] J.-H. Kim, M. Nakamichi, Optimization of synthesis conditions for plasma-sintered beryllium–titanium intermetallic compounds, J. Alloy. Compd. 577 (2013) 90–96.
[13] J.-H. Kim, M. Miyamoto, Y. Hujii, M. Nakamichi, Reactivity and deuterium retention properties of titanium-beryllium intermetallic compounds, Intermetallics 82 (2017) 20–25.
[14] K.A. Walsh, Beryllium Chemistry and Processing, ASM International, 2009.
[15] T.G. Nieh, J. Wadsworth, F.C. Grensing, J.-M. Yang, Mechanical properties of vanadium beryllide, VBe_{12}, J. Mater. Sci. 27 (1992) 2660–2664.
[16] P. Kurinskiy, H. Leiste, A. Goraieb, R. Rolli, S. Mueller, J. Reimann, A. Moeslang, Production of Be-Ti and Be-Zr rods by extrusion and their characterization, Fusion Eng. Des. 136 (2018) 49–52.
[17] G.V. Samsonov, I.M. Vinitskii, Handbook of Refractory Compounds (translated from the Russian by Kenneth Shaw), IFI/Plenum Press, New York, 1980.
[18] J.L. Murray, Beryllium-Titanium Phase Diagram, Phase Diagrams of Binary Beryllium Alloys, ASM International, 1987.
[19] M. Nakamichi, K. Yonehara, Sintering properties of beryllides for advanced neutron multipliers, J. Nucl. Mater. 417 (2011) 765–768.
[20] J.-H. Kim, M. Nakamichi, The effect of sintering time on synthesis of plasma sintered beryllides, J. Nucl. Mater. 442 (2013) 461–464.
[21] J.-H. Kim, M. Nakamichi, Oxidation behavior of plasma sintered beryllium–titanium intermetallic compounds as an advanced neutron multiplier, J. Nucl. Mater. 438 (2013) 218–223.
[22] V. Chakin, R. Rolli, R. Gaisin, P. Kurinskiy, J.-H. Kim, M. Nakamichi, Effect of heat treatment of titanium beryllide on tritium/hydrogen release, Fusion Eng. Des. 137 (2018) 165–171.